Cascade γ decay study of ^{108}Ag following thermal and resonance neutron capture in ^{107}Ag

L. Zanini*
Paul Scherrer Institute, CH-5232 Villigen PSI, Switzerland

F. Corvi
CEC-JRC, Institute for Reference Materials and Measurements, B-2440 Geel, Belgium

H. Postma
Interfaculty Reactor Institute, Delft University of Technology, Mekelweg 15, NL-2629 JB Delft, The Netherlands

F. Bečvář and M. Krtička
Faculty of Mathematics and Physics, Charles University in Prague, V Holešovičkách 2, CZ-180 00 Prague 8, Czech Republic

J. Honzátko and I. Tomandl
Nuclear Physics Institute, Czech Academy of Sciences, CZ-250 68 Řež, Czech Republic
(Received 22 April 2003; published 30 July 2003)

With the aim to obtain information on the $E1$ and $M1$ photon strength functions at γ-ray energies below the neutron separation energy, we studied two-step γ cascades following the capture of thermal neutrons in ^{107}Ag. For this purpose, we undertook an experiment with the dedicated facility for two-step γ cascades at the Řež research reactor. The obtained data were discussed in conjunction with previous results from resonance neutron capture measurements with the same isotope, obtained at the GELINA facility of the Institute for Reference Materials and Measurements. The cascade γ decay of the ^{108}Ag compound nucleus has been simulated with the aid of the Monte Carlo algorithm DICEBOX assuming several models for photon strength functions. To interpret the results of the experiments, the outcome from these simulations was confronted with the observed cascade-related quantities. The results indicate that the $E1$ photon strength function below the neutron binding energy is suppressed with respect to the conventional Brink-Axel model and that the $M1$ and/or possibly $E2$ photon strengths may play an important role in the decay of compound nucleus at excitations below ≈ 3 MeV.

DOI: 10.1103/PhysRevC.68.014320 PACS number(s): 21.10.−k, 23.20.Lv, 25.40.Lw

I. INTRODUCTION

Within the extreme statistical model, embodying Bohr's idea of a compound nucleus [1], the γ decay of highly excited nuclear states can be described by means of the level density together with a set of photon strength functions (PSFs) for various types and multipolarities of emitted γ radiation. According to this model, the partial radiation width $\Gamma_{a\gamma b}$ for the decay from an initial state a with energy E_a, spin J_a, and parity π_a to a final state b is a random variable which follows the Porter-Thomas distribution [2] with an expectation value given by

$$\langle \Gamma_{a\gamma b} \rangle = \frac{f_{XL}(E_\gamma) E_\gamma^{2L+1}}{\rho(E_a, J_a, \pi_a)}, \tag{1}$$

where $f_{XL}(E_\gamma)$ is the PSF for transitions of type X and multipolarity L, while $\rho(E,J,\pi)$ is the density of the nuclear levels with spin J and parity π at energy E.

The electric-dipole PSF is the most important for decay of highly excited states. Several theoretical models exist for this PSF. Of them, the most relevant are as follows.

(i) The Brink-Axel model, described in Refs. [3,4]. This model is based on the principle of the detailed balance between the (n,γ) and (γ,n) reactions, on the validity of Brink's hypothesis [4], and on the assumption of the Lorentzian shape for the electric giant dipole resonance (GDR), which is responsible for the major part of the photoabsorption cross section, see Ref. [5]. According to Brink's hypothesis, the GDR is built not only on the ground state, but also on all excited states, each of these GDRs being of the same shape and size.

(ii) The upgraded models, containing various modifications of the shape of the GDR at its low-energy tail, as described in Refs. [6,7]. In view of the assumed temperature dependence of the GDR in these models, the validity of Brink's hypothesis in its strict formulation is violated in these cases. In fact, all of these models are only phenomenological modifications of the Brink-Axel model.

Compared to the case of $E1$ radiation, the theoretical description of average properties of $M1$ transitions is less developed, also in view of strongly limited experimental data. The most relevant models for $M1$ PSFs are the following: (i) The single-particle (SP) model [8]; (ii) the GDR model, based on the idea that the emission of $M1$ γ rays is governed by the $M1$ spin-flip (SF) resonance, centered at around 7 MeV, see Ref. [9], and on an implicit assumption that this resonance is built upon each excited state [10].

Considerable experimental efforts have been devoted to the study of the PSFs. In the beginning, most of the information on PSFs was obtained from photonuclear reactions, see,

*Email address: Luca.Zanini@psi.ch

for instance, Ref. [6]. So far, the most significant data came mainly from the (n,γ) reaction, their direct source being resonance neutron capture experiments. If the initial state a is a neutron resonance and the final state b is a low-lying state of the product nucleus, an estimate of $\langle\Gamma_{a\gamma b}\rangle$ on the left-hand side of Eq. (1) can be obtained by averaging the experimentally observed partial widths $\Gamma_{a\gamma b}$ of primary transitions over as many resonances a of the same spin and parity as possible. The main limitation of this approach comes from the fact that it is restricted to a relatively narrow energy window; in fact, only primary transitions to the low-lying levels (up to about 2 MeV for even-even medium-heavy nuclei and 1 MeV in other medium-weight or heavy nuclei) can be well resolved.

Intensities of low-energy transitions following neutron capture, together with the total radiation widths, neutron capture cross sections, and the shapes of spectra in the $(n,\gamma\alpha)$ are examples of sources of information on PSFs at γ-ray energies below 4 MeV. However, comparisons of this kind of experimental data with what is expected from predictions using the available models of the PSFs lead in most cases to meaningful conclusions only regarding the $E1$ transitions, see, e.g., Refs. [6,11].

With the aid of the nuclear resonance fluorescence and the (e,e') reaction, significant progress has been achieved during the last decade in studying the low-energy ground-state $M1$ transitions. The observed structure at $E_\gamma \approx 3$ MeV in deformed nuclei has been interpreted in terms of $M1$ scissors mode vibrations. Of great importance are also the results from the (p,p') reaction that provide a strong evidence for the existence of a two-hump $M1$ SF resonance in deformed nuclei. However, serious problems persist in getting reliable information on properties of the $M1$ PSF. It is still difficult to estimate the relative size of this PSF with respect to the $E1$ PSF, as well as its dependence on the γ-ray energy. In particular, considering the SP and SF models for description of the $M1$ PSF at energies $E_\gamma > 4$ MeV, the available experimental data for the majority of nuclei prefer none of the two alternatives. In addition, scarcity of the data on PSFs at energies below 4 MeV leaves the question about the behavior of the $M1$ transitions at these energies virtually unanswered, especially in the case of medium-weight and heavy nuclei.

It is of great interest to carry out an experiment which would be able to distinguish, at least in part, between different characters of radiation in order to isolate the contribution of the $M1$ transitions in (n,γ) reactions. Since the $M1$ transitions are generally weaker than the $E1$ transitions, at least for the higher γ-ray energies, this task is not easy. In recent years, the method of the two-step cascades (TSCs) following thermal-neutron capture, introduced more than 40 years ago by Hoogenboom [12], and rediscovered by the Dubna group [13], has been applied to the study of the PSFs [11,14]. Unlike in other experiments, this technique is able to distinguish, at least to some degree, between the effects from the $E1$ and $M1$ transitions. Specifically, the spectra yielded by the TSC method are sensitive to the relative sizes of the PSFs for multipolarities $E1$ and $M1$ in the γ-ray energy region centered around 2–5 MeV, where virtually all traditional approaches to study PSFs fail.

Also the linear polarization of individual γ-ray transitions emitted after neutron capture by oriented nuclei may reveal information about their $E1$ and $M1$ character, but these experiments need complicated and expensive equipment.

With the purpose to determine which models of the $E1$ and $M1$ PSFs describe better the γ decay of an excited, medium-mass spherical nucleus, we devoted a significant part of this paper to a study of TSCs, following the capture of thermal neutrons in ^{107}Ag. The TSC measurements were performed [15] at the research reactor at Řež. The great advantage of thermal neutrons is their high flux available at reactors, which is an essential requirement for coincidence measurements.

Our previous experiment [16,17], which focused on the spectroscopy of capture γ rays from isolated neutron resonances of the $^{107}\mathrm{Ag}+n$ and $^{109}\mathrm{Ag}+n$ reactions, revealed a distinct dependence of populations of low-lying levels in ^{108}Ag and ^{110}Ag on the parity of the initial neutron capturing state. Specifically, it has been found that the relative intensities of γ transitions from selected low-lying levels of different parity depend strongly on the parity of the initial resonance capturing state with an effect as big as 40%, comparable to that of the well-known spin effect, see Refs. [16–19]. The observation of this unusual phenomenon leads to a constraint on the selection of the $E1$ and $M1$ PSFs, which is independent from that following from the data on TSCs. For this reason, with a perspective of a more accurate determination of the PSFs for ^{108}Ag, the present paper includes a combined analysis of the data on TSCs and the resonance data accumulated on secondary γ transitions [16]. Moreover, neutron resonance data on primary γ rays with $E_\gamma > 6$ MeV from our previous experiment were used to set an additional condition on the ratio of $E1$ to $M1$ PSFs.

The Monte Carlo code DICEBOX [20] has been used to simulate the statistical decay of the compound nucleus ^{108}Ag. Under assumptions of the validity of various models of the PSFs, it was possible to use this code for simulating the γ cascades depopulating the neutron capturing state of the compound nucleus. Analyses of large enough sets of these cascades allowed us to predict the intensities of the most prominent low-energy transitions in ^{108}Ag nucleus and also to construct the spectra of all those TSCs that end at various prefixed final states in this nucleus. These predictions were in turn confronted with their experimentally determined counterparts to accept or reject the considered models of the PSFs.

II. DESCRIPTION OF THE TSC EXPERIMENT

The TSC measurement was performed at the 15-MW light-water reactor at Řež. As a thorough description of the experimental setup and the TSC technique are given in Refs. [14,15], in the following we give only the details specific to the present measurement.

The neutron beam, collimated to a cross section 2.5 $\times 0.25$ cm^2 at the sample position, had a flux of about 3×10^6 cm^{-2} s^{-1}. Neutron capture γ rays were detected by two HPGe detectors, of about 25% efficiency, placed close to the sample to increase the number of coincidences. A sample

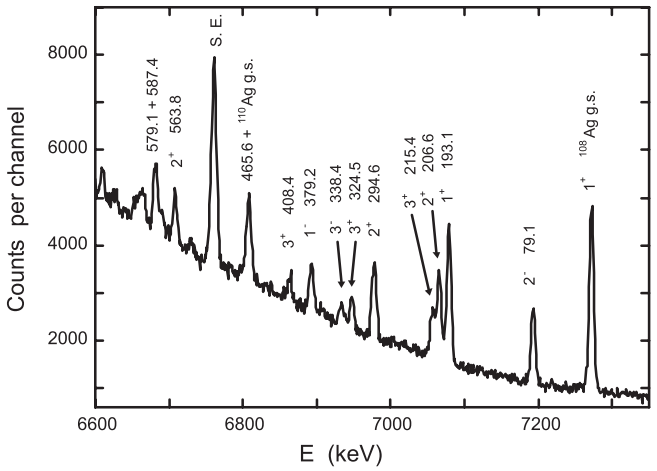

FIG. 1. The energy-sum spectrum for TSCs following the capture of thermal neutrons in a sample of Ag enriched in ^{107}Ag as measured by two Ge detectors in coincidence. Except for one single-escape peak, only the full-energy peaks are labeled. Each of them belongs to all those TSCs that proceed from the capturing state and terminate at a fixed final level in ^{108}Ag. The values of spin and parity of these levels are shown together with level energies, expressed in keV. A possible admixture due to the capture in ^{109}Ag is also indicated.

of silver of 0.2 g, enriched to 99% in ^{107}Ag, was used. The background of capture γ rays from ^{109}Ag was thus considerably reduced. Moreover, because of the lower neutron binding energy of ^{109}Ag compared to ^{107}Ag (6.9 and 7.3 MeV, respectively), there is virtually no background due to capture in ^{109}Ag in the upper part of the energy-sum spectrum. The measurement lasted about 300 h, with an average counting rate of 150 coincidences/s. γ rays in the energy range 0.1–7.3 MeV were recorded.

The resulting spectrum of γ-ray energy sums is shown in Fig. 1. Each of the labeled peaks originates from simultaneous detection of all possible pairs of γ rays belonging to the TSCs that end at a specified final level in ^{108}Ag. With the exception of one single-escape peak, the peaks labeled in Fig. 1 result from the full deposition of γ ray energies in the detector pair. A parasitic contribution from the TSCs terminating at the ^{110}Ag ground state is also indicated.

From the information recorded in the event mode, the spectra of γ rays, belonging to all TSCs that end at preselected final levels in ^{108}Ag, were constructed. These so-called TSC spectra were obtained for nine ^{108}Ag levels, called hereafter TSC final levels, for which the corresponding full-energy peaks in the spectrum of energy sum (Fig. 1) are well resolved, specifically for the 1^+ ground state and the levels at 79.1, 193.1, 294.6, 324.5, 338.4, 379.2, 408.4, and 563.8 keV with spin and parity 2^-,1^+,2^+,3^+,3^-,1^-,3^+, and 2^+, respectively.

While constructing the TSC spectra, the background due to accidental coincidences and Compton scattering was subtracted: Compton background was subtracted choosing background regions on the two sides of each peak in the sum spectrum, as described in Ref. [15]. Time windows, selecting three intervals of detection-time difference, were adjusted to isolate the net signal from the background due to accidental coincidences; for details, see Refs. [14,15]. The TSC spectra were corrected for energy dependence of the full-energy peak efficiencies of both detectors, thus obtaining symmetric spectra in which the area of every peak in the low-energy part is equal to that of the corresponding partner peak at the high-energy side.

TABLE I. Integrated TSC intensities for nine final states (indicated with E_x) of the ^{108}Ag nucleus. The corrections for vetoing effects (f_V) and for angular correlation ($\langle f_{AC}\rangle$) are also listed.

E_x (keV)	J^π	f_V	$\langle f_{AC}\rangle$	$I^{(\mathrm{expt})}$ (γ's/100n)
0	1^+	1	0.93	1.414±0.095
79.1	2^-	1	1.07	1.115±0.080
193.1	1^+	1.01	0.93	1.079±0.075
294.6	2^+	1.06	1.07	0.645±0.069
324.5	3^+	1.02	0.97	0.406±0.050
338.4	3^-	1.05	0.97	0.443±0.051
379.2	1^-	1.07	0.93	0.747±0.067
408.4	3^+	1.05	0.97	0.225±0.055
563.8	2^+	1.08	1.07	0.390±0.066

The efficiency-corrected TSC spectra were further modified by two successive renomalizations in order to compensate the vetoing effects, caused by the detection of γ rays following the decay of a TSC final level, and the role of angular correlation following the procedure, as described in Refs. [11,14]. For this purpose, respective multiplication factors f_V and f_{AC} were determined. We used the explicit expression for the angular-correlation function $W(\Theta)$, as described in Ref. [21]. The size of a correction depends on the spin sequence, on the multipolarity of the γ transitions involved, on the multipolarity mixing ratios, and on an appropriate solid angle correction. The angular-correlation correcting factor f_{AC} was calculated for each final state of interest taking into account all possible spins of the intermediate levels and considering only pure dipole transitions.

Corrections of each peak in the TSC spectrum for angular-correlation effects can be achieved by multiplying the efficiency-corrected spectral intensity of each bin at the TSC spectrum by a corresponding correcting factor, averaged with proper weights over all possible spin values of the intermediate levels involved. The values of the averaged correcting factor $\langle f_{AC}\rangle$, referring to the 2.8-MeV-wide γ-ray energy interval in the middle part of the TSC spectra (see below), are listed in Table I.

As described in Ref. [14], two other types of parasitic phenomena are involved in this kind of measurement. The cases of multistep cascades, when three or more γ rays from one cascade deposit their energies in two detectors, constitute a contribution to the background of the measured TSC events. This contribution can be reasonably well estimated by Monte Carlo simulations. We found that the contribution of three-step cascades reached at most a few percent of the overall integrated TSC intensity, while the contribution of higher multiplicity events was fully negligible.

A γ cross talk between the two detectors should also be taken into account. Parasitic effects due to cross talk were

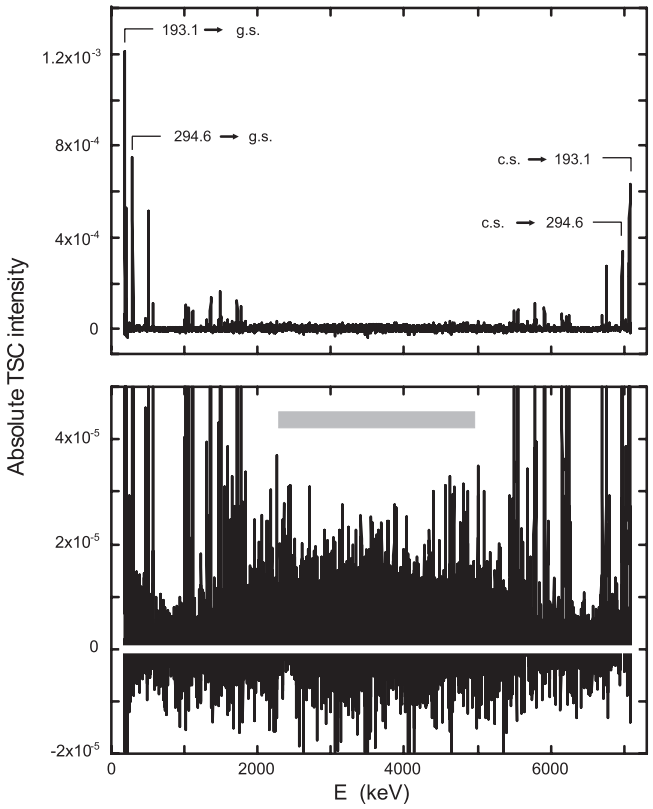

FIG. 2. Symmetrized, background-corrected spectrum of the TSCs terminating at the ^{108}Ag ground state plotted in two different scales. Transitions responsible for the most prominent lines are indicated. The region for getting the integrated TSC intensity is shown in the lower part of the figure.

deeply investigated in Ref. [14]. As in most cases the cross-talk γ rays have very low energy, we strongly reduced these effects by placing 2-mm-thick lead absorbers in front of each detector.

After applying these corrections, the TSC spectra were converted into the spectra of absolute TSC intensities. As a result, the area under each line in a TSC spectrum became equal to the product of two branching ratios for the corresponding pair of the primary and secondary transitions involved. This is also the case for myriads of the unresolved lines from the level quasicontinuum. Conversion of the TSC spectra into units of absolute intensities was performed with the aid of a renormalization that ensures correct intensities for a limited set of strong and well-resolved lines. These lines are related to TSCs proceeding via well-established intermediate levels with branching ratios reliably known from other experiments. An example of the TSC spectrum expressed in absolute units of TSC intensities is given in Fig. 2.

From the renormalized TSC spectra, the absolute spectral intensities in the central part, situated in the quasi-continuum region, were integrated. This part was chosen to be 2.8-MeV wide and centered around the midpoint of the TSC spectra, see Fig. 2. The integrated intensities obtained in this way for the TSC spectra, corresponding to various final states for TSCs, were determined with the acceptable experimental precision and simultaneously with the suppressed influence of the residual Porter-Thomas fluctuations. The integrated TSC intensities thus represent suitable observables that can be confronted with predictions based on various models about PSFs and the level density.

The integrated TSC intensities obtained from the spectra for nine different TSC final levels are given in Table I. The indicated experimental errors include all uncertainties except those associated with the renormalization factor f_n discussed in the following section. In this table, values of average angular-correlation correction factor $\langle f_{AC} \rangle$ and the vetoing correction factor f_V obtained from modeling are also listed. In Sec. V, these data are compared with the results from calculations using different models of PSFs.

III. PRIMARY TRANSITIONS FROM NEUTRON RESONANCES IN ^{108}Ag

In a previous experiment in Geel [16], we measured the spectra of γ rays, following the neutron capture at individual resonances of the system $^{107}\mathrm{Ag}+n$ with the aim to determine the spins and parities of the resonances. In this section, we consider a part of the data that were collected, and concentrate our attention on primary γ transitions from isolated resonances.

The high-energy γ spectra of nine isolated ^{107}Ag *s*-wave resonances with $J=1$ below 800 eV were analyzed. For these strong resonances, the $M1$ transitions that are typically weaker than the $E1$ transitions were above the observability threshold, thus reducing the possibility of a biased estimate of the photon strengths. Since information on spins and parities of low-energy levels of ^{108}Ag up to about 1.2 MeV is available, high-energy transitions of known multipolarity in the energy range from 6.1 to 7.3 MeV could be considered.

The average absolute intensity $\langle I_{\gamma f}^{(XL)} \rangle$ for a transition of type *X* and multipolarity *L* from *s*-wave resonances to a level *f* can be used to calculate the value of the photon strength function at transition energy E_γ,

$$f_{XL}(E_\gamma) = \langle I_{\gamma f}^{(XL)} \rangle \langle \Gamma_\gamma \rangle / (E_\gamma^3 D_{(J)}), \tag{2}$$

where $\langle \Gamma_\gamma \rangle$ is the average total radiation width and $D_{(J)}$ is the average spacing between neighboring resonances with a given spin *J*.

In order to determine the absolute transition intensities $I_{\gamma f}^{(XL)}$ from the measured γ-ray spectra for isolated $J^\pi = 1^-$ resonances, we relied on the known data of secondary transition intensities from the previous thermal neutron capture measurements, as summarized in Ref. [22]. In this context, it is crucial that the spin and parity $J^\pi = 1^-$ of the resonances of interest are identical with J^π of the thermal-neutron capturing state. In essence, our determination of $I_{\gamma f}^{(XL)}$ was based on the notion of Coceva [23] that the sum of absolute intensities of all transitions, populating the ground state, must be equal to 100%.

Inspecting the data in Ref. [22], it is evident that the sum of intensities of all transitions from ^{108}Ag levels below 1 MeV to the ground state and to the isomeric state at 109.4 keV is represented by 137 relative intensity units adopted in Ref. [22]. As for the remaining ground-state transitions, ac-

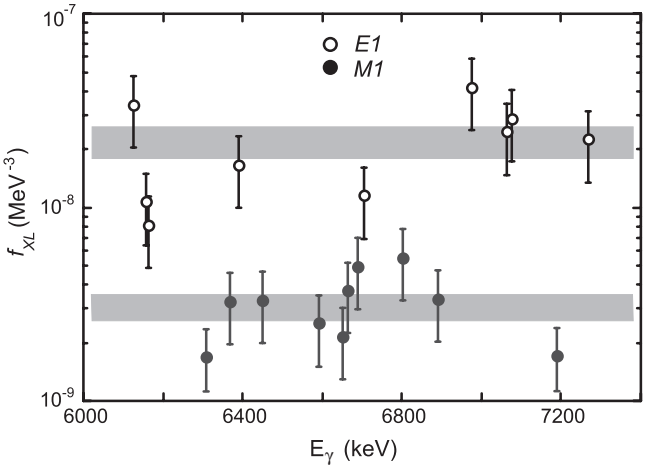

FIG. 3. Experimental average PSFs of $E1$ and $M1$ deduced from the data on primary transitions following the neutron capture in ^{107}Ag at isolated resonances.

cording to our simulations, based on the use of the DICEBOX algorithm [20], transitions from the ^{108}Ag levels in the quasicontinuum above 1 MeV have to contribute to the overall population of the ground state by about 9%. In addition, it has been found from these simulations that the size of the said contribution depends only slightly on the choice of the model combinations for the photon strength functions and the level density. Relying on these ascertainments, we could easily convert the values of relative transition intensities in Ref. [22] into the percentile absolute intensities by merely multiplying the original intensities with a normalization factor $f_n=(100-9)/137$. The uncertainty of this factor is estimated from Ref. [22] to be 10%.

Leaning upon this outlined normalization, we used our data from γ-ray spectra from isolated resonances to determine the average intensities and their uncertainties for primary high-energy transitions. To get these quantities, we applied the maximum-likelihood procedure described in Ref. [24]. The values of the photon strengths are obtained applying Eq. (2); for $\langle\Gamma_\gamma\rangle$ the value of 140 meV from Ref. [25] was used; from the *s*-wave resonance spacing of 25 eV [17], assuming a $2J+1$ dependence of the level density at low spins, the $D_{(1)}$ value of 36.8 eV is obtained. The obtained photon strengths are plotted in Fig. 3.

The average values of the $E1$ and $M1$ strengths in the energy interval between 6.1 and 7.3 MeV are

$$\langle f_{E1}\rangle=(2.19\pm0.35)\times10^{-8}\ \ \mathrm{MeV}^{-3}, \tag{3}$$

$$\langle f_{M1}\rangle=(3.20\pm0.46)\times10^{-9}\ \ \mathrm{MeV}^{-3}. \tag{4}$$

These values, represented by shaded areas in Fig. 3, are in fair agreement with those following from the formulas for the dependence of the photon strengths as a function of the mass number [26].

The indicated uncertainties in the data points of Fig. 3 are only the statistical uncertainties arising from the counting statistics and the assumed Porter-Thomas distribution of the partial radiation widths. Also, contributions from the uncertainties in the average level spacing, the total radiation width, and the normalization factor f_n should be considered, resulting in a larger uncertainty in the average strengths, but by a common factor. However, as far as the ratio between photon strengths $\langle f_{E1}\rangle$ and $\langle f_{M1}\rangle$ is concerned, the role of these additional uncertainties can be neglected. Using the values given in Eqs. (3) and (4), we get

$$\frac{\langle f_{E1}\rangle}{\langle f_{M1}\rangle}=6.9\pm1.5, \tag{5}$$

which is in excellent agreement with the systematics from the literature [27]. We stress the fact that this ratio refers only to transition energies at about 6.5 MeV, and there is no experimental indication that it is valid at lower energies. Nevertheless, it is an important constraint that must be satisfied by the $E1$ and $M1$ PSFs used in the simulations, as discussed in the following section.

IV. NUMERICAL SIMULATIONS OF THE γ DECAY OF THE COMPOUND NUCLEUS ^{108}Ag

For the simulation of the γ decay after neutron capture, the code DICEBOX [20] was used. In this model, the level system of the nucleus and the associated decay scheme are artificially generated according to an adopted level-density model and assumed models of PSFs. However, below some critical energy—in given conditions below 1 MeV—the level energies, spins, parities, and γ-branching ratios are taken from the literature, in our case from Ref. [22]. Hereafter, the generated level structure and the decay scheme are called a *nuclear realization*. While the level structure below the critical energy is kept fixed, many nuclear realizations are generated in a simulation run. For each nuclear realization many γ cascades, initiating at the neutron capturing state and terminating at the ground state, are randomly generated following the rules of the extreme statistical model. Thanks to the introduction of the technique of *precursors*, as described in Ref. [20], the code DICEBOX offers the unique feature of rigorous simulating the residual Porter-Thomas fluctuations of any cascade-related quantity, e.g., the integrated TSC intensities, level populations, population ratios, etc.

In the following, we describe the models of photon strength functions and nuclear level densities that we tested in the simulations.

A. $E1$ photon strength functions

For the $E1$ photon strength functions, we used the standard Brink-Axel (BA) GDR Lorentzian model

$$f_{E1}(E_\gamma)=\frac{1}{3(\pi\hbar c)^2}\frac{\sigma_0 E_\gamma\Gamma_G^2}{(E_\gamma^2-E_G^2)^2+E_\gamma^2\Gamma_G^2} \tag{6}$$

with the parameters $E_G=15.90$ MeV, $\Gamma_G=6.71$ MeV, and $\sigma_0=150$ mb [28]. These parameters are obtained from fitting the photoabsorption data in the energy region from 11 to 20 MeV. In fact, the studied nucleus is probably not ideally spherical. When one tries to fit the photoabsorption data with

double Lorentzian, then the following parameters are obtained: $E_G = 15.03$ and 16.68 MeV, $\Gamma_G = 4.88$ and 7.00 MeV, and $\sigma_0 = 66$ and 96 mb. Nevertheless, the results from the DICEBOX simulations are very similar with both sets of parameters.

Other GDR models exist, which are characterized by a partial violation of Brink's hypothesis, since the GDR changes in shape and size with excitation energy [6,29]. Among them we decided to test the model proposed by Kadmenskij, Markushev, and Furman (KMF) [7], which has been derived in the frame of the semimicroscopic shell-model approach (exploiting the results of the theory of Fermi liquids) in an attempt to describe the behavior of the $E1$ photon strength function at the low-energy tail of the electric GDR. This model is particularly interesting, since it was developed especially for spherical nuclei. Following the KMF model

$$f_{E1}(E_\gamma, T) = \frac{1}{3(\pi\hbar c)^2} F_K \frac{\sigma_0 E_G \Gamma_G \Gamma(E_\gamma, T)}{(E_\gamma^2 - E_G^2)^2}, \tag{7}$$

where

$$\Gamma(E_\gamma, T) = \Gamma_G \frac{E_\gamma^2 + 4\pi^2 T^2}{E_G^2}, \tag{8}$$

$$F_K = \sqrt{\frac{1 + 2f_1/3}{1 + 2f}} \simeq 0.7, \tag{9}$$

f and f_1 are Migdal parameters of the interaction between quasiparticles, see Ref. [7], while T is the nuclear temperature. We also considered the *generalized Lorentzian* (GLO) introduced by Kopecky and Uhl in Ref. [6]. With their approach, the $E1$ PSF is given by the following semiempirical formula valid for spherical nuclei:

$$f_{E1}(E_\gamma, T) = \frac{1}{3(\pi\hbar c)^2} \left[\frac{E_\gamma \Gamma(E_\gamma, T)}{(E_\gamma^2 - E_G^2)^2 + E_\gamma^2 \Gamma(E_\gamma, T)^2} + \frac{F_K \Gamma_G 4\pi^2 T^2}{E^5} \right] \sigma_0 \Gamma_G . \tag{10}$$

Compared to the KMF model, which is, strictly speaking, only a low-energy approximation, the generalized Lorentzian is believed to describe the $E1$ PSF in a wider γ-ray energy region.

The same values of parameters E_G, Γ_G, σ_0 as in the case of the BA model were used in the KMF and GLO models.

The averaged values of the $E1$ PSF evaluated in the energy range between 6.1 and 7.3 MeV are different for these three models. Specifically, the Brink-Axel, KMF, and GLO models lead to the averaged values of $\langle f_{E1} \rangle$ equal to 8.7×10^{-8}, 2.8×10^{-8}, and 1.8×10^{-8} MeV^{-3}, respectively. The KMF and GLO models give reasonable agreements with the above-mentioned experimental result $\langle f_{E1} \rangle = (2.19 \pm 0.35) \times 10^{-8}$ MeV^{-3}, while the prediction of the Brink-Axel model displays a statistically significant departure from this result. This is in agreement with conclusions of Ref. [10] on the neighboring nucleus ^{106}Pd.

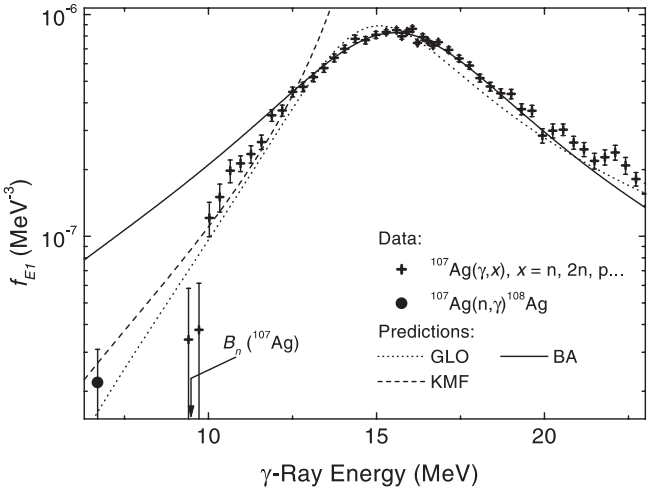

FIG. 4. Comparison of predictions for the $E1$ photon strength function from various models with data from the ^{107}Ag(n,γ) ^{108}Ag reaction (present work) and the photonuclear data for neigboring nucleus ^{107}Ag (Ref. [30]).

In Fig. 4, the photonuclear data on f_{E1} for ^{107}Ag [30] are plotted together with the data from the ^{107}Ag$(n,\gamma)^{108}$Ag reaction reported in this work. One can see that the models with E_γ^2 dependence of the damping width Γ_G describe both kinds of data below 12 MeV significantly better than the BA model with a constant Γ_G.

B. $M1$ photon strength functions

In our analyses, the SP and the Lorentzian SF models for the $M1$ PSF were used. In accordance with data in Ref. [6], the parameters of the spin-flip model were adjusted at values $E_G = 8.61$ MeV and $\Gamma = 4$ MeV. For the remaining parameter, the peak photoabsorption cross section of the spin-flip resonance, we took values of σ_0 which reproduced the above-mentioned ratio $\langle f_{E1} \rangle / \langle f_{M1} \rangle$ at γ-ray energies of 6.1–7.3 MeV. The same constraint on the ratio $\langle f_{E1} \rangle / \langle f_{M1} \rangle$ has been used for the determination of the constant value of f_{M1} embodying the single-particle model. If this constraint includes the $E1$ PSF following from the GLO or KMF models, both outlined $M1$ PSFs will yield values that are fully compatible with experimental values given in Eq. (4). In contrast to this, if the constraint, imposed on $\langle f_{E1} \rangle / \langle f_{M1} \rangle$, relies on predictions of the $E1$ BA model, the $M1$ PSFs will be in a sharp contrast with the experimental values on the right-hand side of Eq. (4). Nevertheless, the model combinations including the BA model have been tested, because this model is widely used. The selected values of σ_0 and f_{M1} for the $M1$ SF and $M1$ SP models, respectively, are given in Table II.

From the available data on intensities of γ transitions between low-energy levels [22,31], it is apparent that the majority of the low-energy transitions have $M1$ character. This may be an index of the importance of the $M1$ strength function for this nucleus, at low-excitation energies. Therefore, in order to account for a possible enhancement of the $M1$

TABLE II. The model combinations used in the simulations. For the $E1$ GDR models, the values for the parameters E_G, Γ_G, and σ_0 were 15.9 MeV, 6.71 MeV, and 0.15 b, respectively. Different values were used for the $M1$ PSFs, in order to respect the $E1$ to $M1$ intensity ratio at high γ-ray energies. They are indicated in parentheses. For the Lorentzian models, the indicated values in the parentheses are the E_G (MeV), Γ_G (MeV), and σ_0 (b), respectively. The single-particle values are in units of MeV^{-3}. For the meaning of the remaining $M1$ and $E2$ models, see explanation in the main text. The experimental value of total radiation width is $\langle\Gamma_\gamma\rangle = 140 \pm 20$ (meV).

Combination	$E1$	$M1$	$E2$	Level density	Γ_γ (meV)
a	BA	BA (8.6; 4; 8×10^{-4})	SP	CTF	156 ± 7
b	BA	SP (1.24×10^{-8})	SP	BSFG	214 ± 7
c	KMF	BA (8.6; 4; 8×10^{-4})	SP	BSFG	103 ± 3
d	KMF	SP (4.0×10^{-9})	SP	BSFG	131 ± 3
e	GLO	SP (2.5×10^{-9})	SP	BSFG	55 ± 1
f	KMF	$f_{M1}^{(1)}(4.0\times10^{-9})$	SP	BSFG	131 ± 3
g	KMF	$f_{M1}^{(2)}(4.0\times10^{-9})$	SP	BSFG	131 ± 3
h	KMF	SP (4.0×10^{-9}) and $f_{M1}^{(3)}$(2; 1; 5; 3)	SP	BSFG	131 ± 3
i	KMF	SP (4.0×10^{-9})	$f_{E2}^{(1)}$(3,100)	BSFG	131 ± 3
j	GLO	$f_{M1}^{(2)}(2.5\times10^{-9})$	SP	BSFG	55 ± 1

strength function, we introduced three simple expressions to enhance the $M1$ strength in the cascades at low-excitation energies.

The first one gives a simple enhancement of the $M1$ strength by a factor K for transitions from levels with excitation energies E below some threshold excitation $E_{\rm thr}$,

$$f_{M1}^{(1)}(E_\gamma;K,E_{\rm thr}) = \begin{cases} K f_{M1}^{SP} & \text{for} \quad E < E_{\rm thr} \ \text{(MeV)} \\ f_{M1}^{SP} & \text{for} \quad E > E_{\rm thr} \ \text{(MeV)}. \end{cases} \tag{11}$$

In our case, we set $E_{\rm thr}=3$ MeV and $K=5$.

The second formula, taken from Ref. [32], assumes above the critical energy of 1 MeV the following dependence of the $M1$ strength on the excitation energy:

$$f_{M1}^{(2)} = f_{M1}^{SP}\frac{B_n}{E}, \tag{12}$$

where B_n is the neutron binding energy and E is the excitation energy.

The third formula is obtained by adding a Lorentzian to the SP strength for transitions initiating at energies below a threshold energy $E_{\rm thr}$. This Lorentzian is referred to as $f_{M1}^{(3)}(E_G,\Gamma,\sigma_0,E_{\rm thr})$. The parameters used are listed in Table II.

C. $E2$ photon strength functions

For the $E2$ PSF, the single-particle model was used in the calculations with the value $f_{E2}^{SP}=5\times10^{-11}$ MeV^{-5}, see Ref. [26].

The γ decay after neutron capture is usually dominated by the $E1$ and $M1$ transitions [33]. However, some experimental evidence exists [34] that the $E2$ PSF could be enhanced by a large factor at low nuclear excitation energies; therefore also in this case we introduced a very crude *ad hoc* PSF denoted $f_{E2}^{(1)}$. This model enhances the f_{E2}^{SP} by a factor 100 below 3 MeV.

D. Nuclear level densities

We used two common, parity-independent, models of nuclear level density. The first one is represented by the constant temperature formula (CTF)

$$\rho(E,J) = \frac{f(J)}{T}\exp\left(\frac{E-E_0}{T}\right), \tag{13}$$

where E_0 and T can be adjusted to fit with experimental data at low-excitation energies and in the region of neutron resonances; $f(J)$ is the spin distribution factor:

$$f(J) = \exp\left(\frac{-J^2}{2\sigma_c^2}\right) - \exp\left(\frac{-(J+1)^2}{2\sigma_c^2}\right), \tag{14}$$

where σ_c is the spin cutoff factor given by $\sigma_c \simeq 0.98A^{(0.29)}$, see Ref. [35].

The second model is the backshifted Fermi gas (BSFG) model [36]:

$$\rho(E,J) = f(J)\frac{e^{2\sqrt{a(E-E_1)}}}{\sigma_c 12\sqrt{2}a^{1/4}(E-E_1)^{5/4}}, \tag{15}$$

where again a and E_1 can be adjusted to experimental data. The spin cut-off factor is given in this case by the formula in Ref. [37],

$$\sigma_c^2 = 0.0888A^{2/3}\sqrt{a(E-E_1)}. \tag{16}$$

The parameters in Eqs. (13) and (15) are taken from Ref. [35]. Specifically, $a=13.76$ MeV^{-1}, $T=0.748$ MeV, $E_0=-2.52$ MeV, and $E_1=-1.08$ MeV. According to several theoretical indications [38–40], nuclear level densities are expected to exhibit dependence on the parity of the levels up to several MeV of excitation energy. However, as there was no explicit expression for the level-density formula displaying a parity asymmetry that would be applicable for ^{108}Ag, we tested only the above-mentioned models.

In Table II, the model combinations used in this paper are listed. We chose the model combinations with the constraint that the average total radiation width $\langle\Gamma_\gamma\rangle$ be close to the average experimental value of 140 meV [25]. It is noted that this requirement ruled out some possible model combinations. For instance, keeping in mind that each model combination should also predict correctly the ratio $\langle f_{E1}\rangle/\langle f_{M1}\rangle$ for high-energy γ rays, see Sec. III, the standard $E1$ GDR model for the PSF combined with the $M1$ SP model and the CTF level density (which predicts fewer levels and thus smaller total radiation width than the BSFG) leads to the average width $\langle\Gamma_\gamma\rangle$ of about 300 meV, which exceeds significantly the corresponding experimental value. For this reason the combination of the $E1$ GDR with the $M1$ SP is not included in Table II. Nevertheless, since we were very interested in testing the predictions given by the GLO model for the $E1$ PSF, we included two model combinations incorporating this model, although the calculated value of $\langle\Gamma_\gamma\rangle$ is too small, only 55 meV.

E. Simulations

For each of the considered model combinations, the γ-cascade process for resonances with different spins and parities was simulated performing DICEBOX runs, with the initial spins and parities $J^\pi=0^-,1^-,0^+,1^+,2^+$. For each run we simulated 50 000 events in each of the 50 nuclear realizations, that is, for a total of 2.5×10^6 events.

In order to analyze the data from isolated neutron resonances, the cascade-related quantities simulated with the aid of the DICEBOX algorithm were the intensities of the low-energy γ transitions and the γ multiplicity. For the need of interpretation of the data from the TSCs, following the decay of the thermal-neutron capturing state $J^\pi=1^-$ in ^{108}Ag, our simulations included also the integrated TSC intensities. In this connection, it is noted that the contribution of the other s-wave capturing state, $J^\pi=0^-$, was considered to be negligible.

V. RESULTS FROM CALCULATIONS

A. General remark on uncertainties of the evaluated quantities

The uncertainties shown below include contributions from the statistical uncertainties, from the Porter-Thomas fluctuations and, in the case of resonances, from the uncertainty on the experimental branching ratios.

As previously mentioned, a critical energy of 1 MeV was chosen, below which the energy, spin, and parity of low-energy levels are assumed to be known from the literature. The critical energy is somewhat arbitrarily chosen as a value below which the information about the levels is believed to be complete or almost complete with few levels or none of the levels missing. In the case of ^{108}Ag, there are a few levels below the accepted critical energy of 1 MeV with two or more spin and/or parity values given. In most cases, changing the spin or parity value of a level with incomplete information does not affect significantly the results of the calculations for the integrated TSC intensities. On the other hand, changing spin or parity values of a level may affect the calculated intensities of low-energy transitions. In general, if a γ transition originates from a level with known spin, changing the spins of upper energy levels which feed this level may affect the calculated intensity by about 10–20 % at most. The same is true if the level from which the γ transition originates has unknown spin but the possible spins have low values, such as 1 or 2. If, on the contrary, a γ transition comes from a level with higher spin and more than one value is available from literature, the differences in the calculated intensities can vary a lot with the spin. One example is the 485.1-keV level for which two possible spins, 4 or 5, are given in Ref. [22]. This is an important level because it generates the line of 329.2 keV, which was used for the resonance spin assignment (see below). Changing the spin value from 4 to 5 gives a decrease of the intensity of the 329.2-keV line by a factor 20, almost independently on the model combination used in the calculations. This big difference is due to the fact that a level with $J=4$ can be reached by three-step dipole cascades from the capturing thermal state, while a $J=5$ level can be reached only by cascades with four or more steps, which are much less likely. In this case we accepted $J=4$ for the level, because the intensity of the 329.2-keV line calculated with the help of the DICEBOX simulations is very close to the experimental value from thermal-neutron capture.

B. Resonance neutron capture

1. Spin effect

The dependence of the intensities of the low-energy γ rays on the spin of the capturing state is a well-known effect, which is due to two characteristics of the γ-cascade decay: the low-average multiplicity, and the prevailing dipole character of the emitted γ radiation. With the exception of the model combination i), which includes a strong $E2$ enhancement, these two characteristics are inherent to all combinations listed in Table II. A strong spin dependence of the γ-ray intensities of transitions between low-lying levels is, therefore, anticipated. The validity of a given model combination can be thus assessed from the size of the spin effect that it predicts.

In Ref. [16], the intensity ratio of γ transitions with energies 300.1 and 329.2 keV, deexciting the levels at 379.2 keV ($J^\pi=1^-$) and 485.1 keV ($J^\pi=4^-$), respectively, was used to assign the spin of ^{107}Ag s- and p-wave resonances. In Fig. 5, the calculated values of this ratio for the different model combinations are compared with the experimental values, which represent the averages from several resonances. Specifically, the sets, incorporating 6, 23, 2, 11, and 11 resonances with the respective spin and parity $0^-,1^-,0^+,1^+$, and 2^+, were used for getting the average intensities.

The results of this comparison are summarized in columns 2 and 3 of Table III and visualized in Fig. 5. In calculating the weighted squared deviations S^2 between the modeled and experimentally measured intensity ratios $I(300.1)/I(329.2)$, see Table III, the statistical weights were determined from experimental errors combined with the uncertainties due to the residual Porter-Thomas fluctuations, as determined from

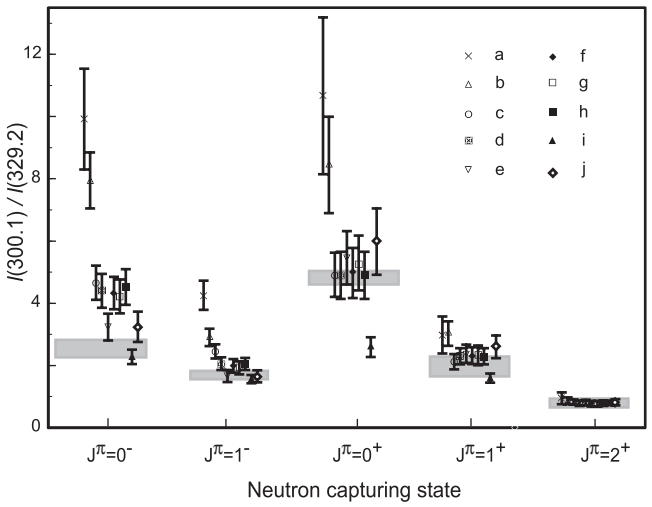

FIG. 5. The spin effect in the reaction ^{107}Ag$(n,\gamma)^{108}$Ag at isolated neutron resonances. The sizes of this effect, predicted from various model combinations of PSFs, are compared with its experimental value (gray bands). The nomenclature used for the individual model combinations is identical to that used in Table II.

the DICEBOX simulations. As expected, all the model combinations considered give a spin effect. However, looking at Fig. 5 and Table III, it is evident that model combinations a)–c) and i) are reliably ruled out. In cases of the remaining model combinations, the predicted values of intensity ratio reproduce qualitatively the behavior of the corresponding experimental values. As seen, the analysis of the weighted square deviations S^2 indicate that the validity of model combinations d) and f)–h) can be ruled out with a significance of 95–99 %, so that they seem to be at the margin of acceptability. In contrast to this, the predicted values from combinations e) and j) lead to almost a perfect accord with the measured intensity ratios. However, these two combinations should be rejected on the basis of the predicted small total radiation width.

From these results, it follows that the data on spin and parity dependence of the intensity ratio $I(300.1)/I(329.2)$ categorically reject the BA model for the $E1$ PSF, leaving at the same time the question about the validity of the GLO model and of the KMF model in its original form open.

2. Parity effect

Contrary to the spin effect, the dependence of γ-ray intensities of transitions between low-lying levels on the resonance parity is still not sufficiently studied, and so far it has been observed only in ^{107}Ag and ^{109}Ag resonance capture [16]. The intensity ratio $R=[I_\gamma(259.3)+I_\gamma(300.1)]/I_\gamma(294.6)$ was used in Ref. [16] to assign the resonance parities. The first two transitions depopulate negative parity levels (338.4 keV with $J^\pi=3^-$ and 379.2 with $J^\pi=1^-$, respectively), while the third transition initiates at the level at 294.6 keV with $J^\pi=2^+$. As evident from experimental data in Ref. [17], this ratio is to a large extent independent of the resonance spin. The independence was confirmed also from the DICEBOX simulations. Therefore, the parity effect can be studied by analyzing the quantity $\langle R_p\rangle/\langle R_s\rangle$, where $\langle R_s\rangle$ and $\langle R_p\rangle$ are intensity ratios R averaged separately over the s-wave resonances with $J^\pi=0^-,1^-$ and p-wave resonances with $J^\pi=0^+,1^+,2^+$, respectively.

As is evident, combinations a)–c) are three to four standard deviations from the experimental value $\langle R_p\rangle/\langle R_s\rangle=1.51\pm0.15$ and can, therefore, be rejected. The remaining model combinations yield parity effects in the right direction and with values in reasonable accord or fully compatible with the experimental value (Fig. 6). The model combinations giving the highest parity effect are the ones which involve enhancement of the $M1$ or $E2$ strength at low γ-ray energies. As we already mentioned, the combinations e) and

TABLE III. The sums S^2 of the statistically weighted squares of deviations between the observed quantities and their modeled counterparts are listed for various types of quantities studied and various model combinations. For each value of S^2, the probability $P(\chi^2<S^2)$ that the χ^2 random variable for a specified number of degrees of freedom ν is lower than S^2 is also given. Values of S^2 for which the corresponding probability is lower than 0.99 are underlined. In addition, this table lists coefficients r of linear correlation between the modeled and the measured integrated TSC intensities.

	Observable						
	$I(300.1)/I(329.2)$		$\langle R_p\rangle/\langle R_s\rangle$		Integrated TSC intensity		
Model	($\nu=5$)		($\nu=1$)		($\nu=9$)		
combination	S^2	$P(\chi^2<S^2)$	S^2	$P(\chi^2<S^2)$	S^2	$P(\chi^2<S^2)$	r
a	61.4	>0.9999	16.6	>0.9999	97.2	>0.9999	0.51
b	65.8	>0.9999	9.7	0.9982	38.4	>0.9999	0.92
c	26.2	0.9999	11.2	0.9992	56.4	>0.9999	0.71
d	15.6	0.9916	3.6	0.942	11.7	0.83	0.98
e	4.6	0.53	2.5	0.889	14.5	0.93	0.97
f	13.7	0.981	0.7	0.597	20.4	0.991	0.93
g	11.4	0.958	0.1	0.248	23.3	0.997	0.93
h	15.9	0.972	4.0	0.955	17.1	0.973	0.96
i	21.7	0.9995	0.5	0.520	32.7	>0.9999	0.93
j	6.0	0.704	3.0	0.917	9.8	0.721	0.97

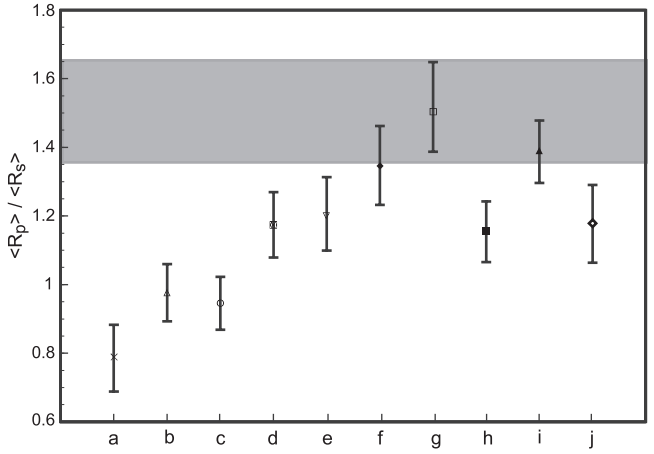

FIG. 6. The parity effect in the reaction $^{107}\mathrm{Ag}(n,\gamma)^{108}\mathrm{Ag}$ at isolated neutron resonances. The sizes of this effect, predicted from various combinations of models for PSFs, are compared with their experimental values (gray bands). For the nomenclature used, see Table II.

j) can be rejected on the basis of the predicted small total radiation width. In addition, d) and i) can be rejected with high statistical confidence on the basis of the spin effect; see columns 2 and 3 of Table III. At this point it is clear that on the basis of the resonance data, model combinations f)–h) based on the KMF model appear to be the most acceptable.

3. Distribution of multiplicities

Although we do not have direct information from the present experiments on the γ-multiplicity distribution, with DICEBOX we could simulate it. In Fig. 7, the calculated multiplicity distributions using model combination d) are shown for different spins and parities of the neutron capturing state. As can be seen, the multiplicity distribution is expected to be only slightly dependent on the spin and parity of the neutron capturing level. This conclusion is in accordance with what has been found by Coceva it et al. [41] from simulations of multiplicity distribution for product nuclei ^{96}Mo, ^{102}Ru, ^{106}Pd, and ^{178}Hf.

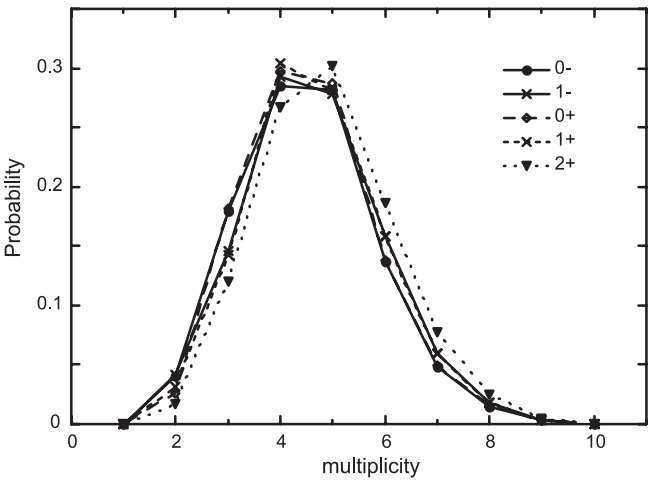

FIG. 7. Distributions of multiplicity of γ cascades following the reaction $^{107}\mathrm{Ag}(n,\gamma)^{108}\mathrm{Ag}$ at isolated neutron resonances, as obtained from simulations within the model combination d), see Table II. The curves shown belong to various values of spin and parity of the neutron capturing state.

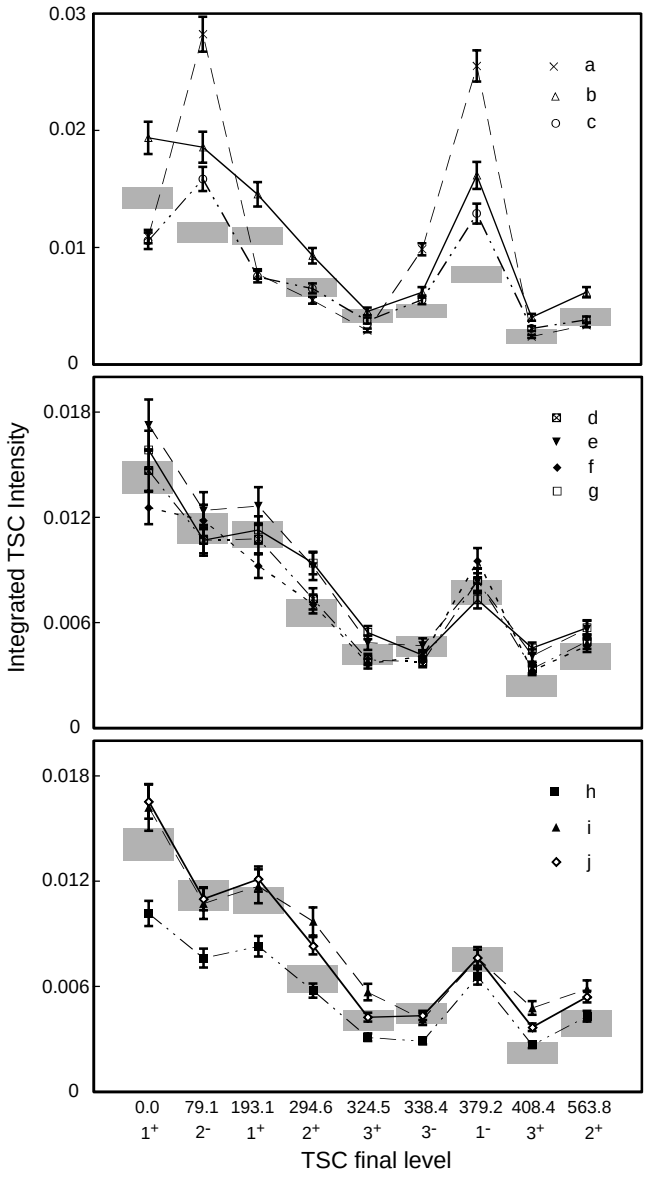

FIG. 8. Comparison between experimental integrated intensities of TSCs (gray bands), following the capture of thermal neutrons in ^{107}Ag, and their values coming from simulations within various combinations of models for PSFs. The integrated TSC intensities are presented in absolute units, i.e., in the number of emitted γ rays that proceed via the selected 2.8-MeV-wide central interval per one neutron capture.

C. Thermal-neutron capture

We calculated the integrated TSC intensities and compared them with the experimental results from Table I. The outcome of this comparison for ten considered model combinations is summarized in columns 6–8 of Table III and illustrated in Fig. 8. Regarding the values of S^2 in column 6,

it is to be stressed that they include not only the experimental uncertainties σ_i of $I_i^{(\mathrm{expt})}$, but also those resulting from *correlated* residual Porter-Thomas fluctuations of the modeled intensities. The elements of covariance matrix V_{ij} needed for this purpose were estimated from simulations based on the DICEBOX algorithm [20].

In order to take into account also the uncertainty σ_Q in intensity normalization factor Q, the weighted square deviation S^2 was in this case taken as

$$S^2=\sum_i \sum_j C_{ij}^{-1}(I_i^{(\mathrm{mod})}-I_i^{(\mathrm{expt})}\,Q)(I_j^{(\mathrm{mod})}-I_j^{(\mathrm{expt})}\,Q) + \overline{Q}^{-1}\frac{1}{\sigma_Q^2}(Q-\overline{Q})^2, \tag{17}$$

where $I_i^{(\mathrm{mod})}$ and $I_i^{(\mathrm{expt})}$ are modeled and experimental integrated TSC intensities, C^{-1} is an inverse matrix to the matrix $C_{ij}=V_{ij}+\sigma_i\delta_{ij}$, and the $\overline{Q}$ is the expected value of normalization factor. The uncertainty σ_Q was assumed to be 10% of $\overline{Q}$. It is expected that S^2 is distributed as χ^2 with eight degrees of freedom.

According to the values of the coefficient r of linear correlation between the measured and predicted integrated TSC intensities, see Table III, the majority of the model combinations reproduce the overall picture, displayed by the experiment. This is also seen from Fig. 8.

Inspecting the values of S^2 and the corresponding probabilities $P(\chi^2<S^2)$ for the integrated TSC intensities, it is clear that combinations a)–g), and i) can be rejected. Although e) and j) are acceptable concerning the integrated TSC intensities, they should be rejected on the basis of the total radiation width. Remaining as more or less acceptable combinations for the integrated TSC intensities are d) and h). Again, the applicability of the BA model is denied, while the KFM model appears to be acceptable in combination with some models for the $M1$ PSF.

Interesting information on the ratio f_{E1}/f_{M1} at low γ-ray or excitation energy ($\approx$3 MeV) can be gained from the comparison of integrated TSC intensities for final 1^- and 2^- levels with those for levels with positive parities. In fact, the integrated TSC intensities for these negative parity levels change drastically and show agreement with experimental values by introducing the considerable $M1$ strength compared to $E1$ strength at low energy. It implies that at low energies ($\approx$3 MeV), the ratio f_{E1}/f_{M1} is different from that ratio at the capture energy of 6.5 MeV. The $M1$ strength appears to play not a marginal but very important role in the decay of the ^{108}Ag compound nucleus (and maybe in nearby nuclei). On the other hand, results from integrated TSC intensities are less sentitive to the photon strength functions at lower-excitation energies: we note that strong enhancements of the $M1$ strength below 3 MeV do not affect the results dramatically, see Fig. 8. Drawing these conclusions it is tacitly assumed that all underlying assumptions of the extreme statistical model of nuclei hold strictly, including the assumption embodied by the concept of photon strength functions.

VI. CONCLUSIONS

A. Nuclear level density

According to our simulations, the TSC intensities as well as J- and π-dependent intensity ratios are not very sensitive to the detailed shape of the level-density function $\rho(E,J)$. In spite of this finding, out of the two models of nuclear level density tested, the backshifted Fermi gas model seems clearly to be preferred over the constant temperature formula in view of predictions imposed on the total radiation width.

B. Photon strength functions

The method of TSCs is confirmed to be an experimental technique sensitive to radiation of different multipolarities in a not well-explored γ-ray energy region of 2–5 MeV. In the present work, we have integrated the results from the TSC experiment with those from the measurements of complementary cascade-related quantities at isolated neutron resonances, specifically the J- and π-sensitive intensity ratios.

The most important results obtained can be summarized as follows.

(i) Clearly the Brink-Axel model for the $E1$ PSF has to be rejected, since it fails to predict the size of any of the observed effects. The $E1$ PSF must be suppressed significantly with respect to this model for γ-ray energies up to about 11 MeV. No experimental data seem to be in contradiction with the E_γ^2 dependence of damping width $\Gamma(E_\gamma,T)$ of the Lorentzian curve.

(ii) The influence of the $M1$ strength on the decay is more important than that predicted with the pure spin-flip mode. This model does not predict almost any $M1$ strength at energies below 5 MeV. Our observations indicate that the $M1$ strength is comparable to the $E1$ strength near 3 MeV. In order to explain the spin and parity dependence of the populations of low-energy levels, observed in resonance neutron capture, one is even forced to assume that the $M1$ strength function is more important than $E1$ at low-excitation region, that is, below about 2 MeV.

As an alternative explanation of the spin and parity effect, a strong enhancement of the $E2$ transitions could be also considered. However, the results from DICEBOX with an $E2$ enhancement are not as successful as that with the $M1$ enhancement, especially as far as the spin effect is concerned.

Within the frame of the considered model combinations, it is very difficult to arrive at predictions that would be in a full harmony with data on *all* available observables, i.e., with (i) the integrated TSC intensity, (ii) the J-dependent intensity ratio $I(300.1)/I(329.2)$, (iii) the π-dependent ratio $\langle R_p\rangle/\langle R_s\rangle$, (iv) the intensities of $E1$ primary transitions, and (v) the total radiation width.

As is evident from Table III, only the model combinations e) and j) are in reasonable agreement with the observables (i), (ii), and (iii). On the other hand, these two models predict a value of the total radiation width which is much too small. Considering only models which predict a realistic total radiation width, models f) and h) appear to be the most acceptable. If a model combination is correct, all three values of $P(\chi^2<S^2)$, listed in Table III, will behave as random num-

bers drawn independently from a uniform distribution in interval (0,1). However, as follows from the binomial distribution, in the case of model f), the probability that two of such random numbers are equal to or greater than 0.981 is only 0.1%. The model combination f) can thus be rejected at the significance level of 99.9% Similarly, the model combination h) can be rejected with statistical significance of 99.99%.

The following explanations of this assessment are possible.

(i) The differences between the modeled and measured quantities are due to too simple model combinations used. In view of the intricate way in which any model combination is responsible for the wide scale of observables, our approach based on searching for a suitable *ad hoc* or phenomenological model combination cannot guarantee successful remedy.

(ii) The process of fragmentation of the photon strength is not governed by Porter-Thomas fluctuations, although the expectation values themselves are strictly obeying predictions following from Eq. (1).

(iii) Predictions of partial radiation widths $\Gamma_{a\gamma b}$ and thus all observables are perturbed by contributions of unknown nonstatistical effects due to a specific structure of the initial and final levels a and b.

(iv) The paradigm of the photon strength functions is not fully justified; in other words, the expectation values of partial radiation widths $\langle\Gamma_{a\gamma b}\rangle$ cannot be represented by a smooth function of E_γ or E_γ and E_a.

Notwithstanding the above-outlined difficulties, the extreme statistical model and the concept of photon strength functions are able to describe the general behavior and virtually all main trends of all observables studied.

We can conclude that the investigation outlined in the present paper constitutes a valid method for getting important information on photon strength functions as well as about spin and parity assignment of neutron capturing states and low-lying levels in medium-weight and heavy nuclei. It is to be stressed that the method of two-step cascades represents the approach which is, to our knowledge, presently the only available method that makes it possible to separate to some degree the contributions from the $E1$ and $M1$ PSFs to the observed effects at intermediate γ-ray energies of 2–5 MeV.

The combination of measurements in resonance and thermal capture allows us to select models in a more definite way than by performing only one measurement, being at the same time sensitive to different ranges of γ-ray energies.

We hope these results will stimulate further theoretical and experimental investigations in order to clarify still persisting open problems.

ACKNOWLEDGMENTS

This work was performed at the Nuclear Physics Institute of Řež, Czech Republic, supported by the grant Agency of the Czech Republic (Grant Nos. 202/97/k038 and 202/03/P136), and at the Institute of Reference Materials and Measurements of Geel, Belgium. One of the authors (L.Z.) would like to thank A. Sukhovoj for useful discussions.

[1] N. Bohr, Nature (London) **137**, 344 (1936).
[2] C.E. Porter and R.G. Thomas, Phys. Rev. **104**, 483 (1956).
[3] P. Axel, Phys. Rev. **126**, 671 (1962).
[4] D. M. Brink, Ph.D. thesis, Oxford University, 1955.
[5] M. Goldhaber and E. Teller, Phys. Rev. **74**, 1046 (1948).
[6] J. Kopecky and M. Uhl, Phys. Rev. C **41**, 1941 (1990), and references therein.
[7] S.G. Kadmenskij, V.P. Markushev, and V.I. Furman, Yad. Fiz. **37**, 277(1983) [Sov. J. Nucl. Phys. **37**, 165 (1983)].
[8] G.A. Bartholomew, Annu. Rev. Nucl. Sci. **11**, 259 (1961).
[9] A. G. Bohr and B. R. Mottelson, *Nuclear Structure* (Benjamin, London, 1975), Vol. II, p. 636.
[10] J. Kopecky and R.E. Chrien, Nucl. Phys. **A468**, 285 (1987).
[11] F. Bečvář, P. Cejnar, J. Honzátko, K. Konečný, I. Tomandl, and R.E. Chrien, Phys. Rev. C **52**, 1278 (1995).
[12] A.M. Hoogenboom, Nucl. Instrum. **3**, 57 (1958).
[13] S.T. Boneva, E.V. Vasileva, Yu.P. Popov, A.M. Sukhovoj, and V.A. Khitrov, Part. Nuclei **22**, 479 (1991).
[14] F. Bečvář, P. Cejnar, R.E. Chrien, and J. Kopecky, Phys. Rev. C **46**, 1276 (1992).
[15] J. Honzátko, K. Konečný, I. Tomandl, J. Vacík, F. Bečvář, and P. Cejnar, Nucl. Instrum. Methods Phys. Res. A **376**, 434 (1996).
[16] L. Zanini, F. Corvi, H. Postma, and F. Bečvář, Phys. Rev. C **61**, 054616 (2000).
[17] L.Y. Lowie *et al.*, Phys. Rev. C **59**, 1119 (1999).
[18] F. Corvi and M. Stefanon, Nucl. Phys. **A223**, 185 (1974).
[19] F. Gunsing, K. Athanassopulos, F. Corvi, H. Postma, Yu.P. Popov, and E.I. Sharapov, Phys. Rev. C **56**, 1266 (1997).
[20] F. Bečvář, Nucl. Instrum. Methods Phys. Res. A **417**, 434 (1998).
[21] K.S. Krane and R.M. Steffen, Phys. Rev. C **2**, 724 (1970).
[22] J. Blachot, Nucl. Data Sheets **81**, 599 (1997).
[23] C. Coceva, Nuovo Cimento Soc. Ital. Fis., A **107**, 85 (1994).
[24] C. Coceva, F. Corvi, P. Giacobbe, and M. Stefanon, Nucl. Phys. **A170**, 153 (1971).
[25] S. F. Mughabghab, M. Divadeenam, and N. E. Holden, *Neutron Cross Sections* (Academic, New York, 1981).
[26] J. Kopecky, in *Neutron Capture Gamma-Ray Spectroscopy*, edited by T. von Egidy *et al.* (Institute of Physics, University of Reading, Berkshire, 1981), p. 426.
[27] L. M. Bollinger, in *Experimental Neutron Resonance Spectroscopy*, edited by J. A. Harvey (Academic, New York, 1970).
[28] B.L. Berman and S.C. Fultz, Rev. Mod. Phys. **47**, 713 (1975).
[29] R. E. Chrien, in *Proceedings of the Fifth International School on Neutron Physics*, edited by Yu. P. Popov (Alushta, Dubna, 1987).
[30] B.L. Berman *et al.*, Phys. Rev. **177**, 1745 (1969).
[31] T.D. MacMahon *et al.*, J. Phys. G **11**, 1231 (1985).
[32] I. Tomandl, Ph.D. thesis, Prague, 1998.
[33] H. Postma, Phys. Rev. C **24**, 2322 (1981).
[34] P. Cejnar and J. Kern, in *Capture Gamma-Ray Spectroscopy*,

edited by J. Kern (World Scientific, Singapore, 1994), p. 542.
[35] T. von Egidy, H.H. Schmidt, and A.N. Behkami, Nucl. Phys. **A481**, 189 (1988).
[36] T.D. Newton, Can. J. Phys. **34**, 804 (1956).
[37] A. Gilbert and A.G.W. Cameron, Can. J. Phys. **43**, 1446 (1965).
[38] S. Hilaire, Ph.D. thesis, Institut National Polytechnique de Grenoble, 1997.
[39] N. Cerf, Nucl. Phys. **A554**, 85 (1993).
[40] B. Pichon, Nucl. Phys. **A568**, 553 (1994).
[41] C. Coceva, F. Corvi, P. Giacobbe, and G. Carraro, Nucl. Phys. **A117**, 586 (1968).